UKAEA FUS 507

EURATOM/UKAEA Fusion

Prospects for Edge Current Measurements on JET - Final Report

NC Hawkes, AA Korotkov, WP Zwingmann, E Rachlew

January 2004

EURATOM/UKAEA Fusion Association

Culham Science Centre
Abingdon
Oxfordshire
OX14 3DB
United Kingdom

Telephone: +44 1235 464181
Facsimile: +44 1235 466435

UKAEA Fusion
Working in Europe

Prospects for Edge Current Measurements on JET
Final Report

N C Hawkes, A A Korotkov, W P Zwingmann†, E Rachlew*

Euratom/UKAEA Fusion Association Culham Science Centre, Abingdon, Oxon, OX14 3DB, UK.

† Euratom/CEA Association, DRFC, CEN Cadarache, F-13108 Saint-Paul-Lez-Durance, France

* Euratom/VR Association, Dept Physics, KTH, Albanova, 10691 Stockholm, Sweden

UKAEA FUS 507

6 Jan 2004

1 Introduction

In a future burning plasma experiment, in order to achive fusion conditions in the machine size envisioned, the experiment may well be required to operate in the H-mode. A serious drawback to this scenario is the occurrence of large, type-I, ELMs which would lead to rapid erosion of the divertor target plates. Therefore, the desired operating scenario relies on producing small, type-III, ELMs by controlling the edge parameters, and in particular by preventing the edge plasma from accessing the second region of ballooning stability.

In order to be confident of establishing such an operating condition in a future experiment we must achieve a good understanding of the edge region of H-mode plasmas in present experiments. Crucial to this understaning is the measurement of the edge current density profile. In H-mode, significant current density is driven by bootstrap in a narrow region in the transport barrier. This current modifies the ballooning stability boundary and can, in principle, allow this part of the plasma to access the second stability region.

The necessary complement to the measurement of the edge current density is the accurate determination of the edge pressure profile. This has an indirect influence on the stability boundary, via the equilibrium, but is of direct importance in locating this plasma region in s-α coordinates.

1.1 Measurement Options

The important parameters in the study of transport and stability at the plasma edge (indeed at any position in the plasma) are the current profile density $J(R)$ and the radial electric field E_r. These quantities are both involved in the supression of turbulence (E_r flow shear, magnetic shear) and stability ($J(R)$). Other than material probes, there are three techniques used to measure these quantites, none of which provides a direct measurement:

Impurity Charge Exchange is used to measure E_r but is an indirect measurement that evaluates E_r from the zero order radial force balance for impurities (usually carbon). The measurement provides the impurity pressure gradient and

the toroidal and poloidal flow velocities. From these measurements E_r can be calculated.

Zeeman Polarimetry or Ratiometry provide information on the magnetic field line direction, independent of the plasma electric field. Zeeman polarimetry measures the polarisation direction of light emitted from neutral lithium atoms injected into the plasma. The polarisation is aligned with the direction of the local magnetic field; the global magnetic field geometry and current density profile are obtained from a solution of the magnetic equilibrium equation using input from other magnetic sensors. Zeeman Ratiometry is the measurement of the relative intensities of the σ and π components of the resonance multiplet emitted by lithium atoms. The ratio gives the direction of the local magnetic field vector while the magnitude of the total magnetic field can be determined from the multiplet splitting[1].

Motional Stark Effect Polarimetry (MSE) is similar to Zeeman polarimetry, but measures the local electric field vector in the frame of fast injected deuterium atoms (often from the heating neutral beams). The electric field is the sum of the contributions from the beam atom motion and that (smaller contribution) due to the plasma[2]. The interpretation of these measurements requires the same analysis as that of Zeeman polarimetry as well as requiring the information from charge exchange to correct the contribution from the plasma E_r.

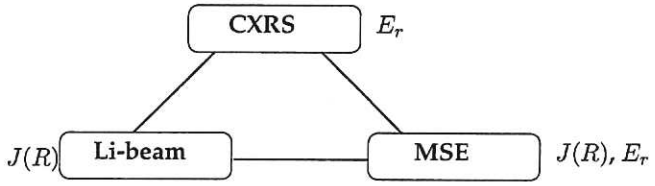

A full characterisation of the edge plasma therefore requires the implementation of two of the above techniques.

1.1.1 MSE

In JET, in the core plasma, the MSE diagnostic provides measurements of the magnetic field pitch angle, and hence the current density profile, with a space resolution of 5 cm. MSE measurements are influenced by the plasma radial electrostatic field, E_r[1], and in the region of the H-mode transport barrier these fields are sufficently strong ($> 60\,k\text{V.m}^{-1}$)[2] as to have a serious impact on the MSE measurements. In principle the influence of these fields can be compensated, but this requires a full characterisation of the edge region (measurement of all the terms of the radial force balance equation, pressure gradient, toroidal and poloidal flow velocities) and accurate mapping between the various edge measurements.

The best precision measurements with the edge charge exchange system yield errors in the flow velocity components of $20\,\text{kms}^{-1}$ toroidally and $10\,\text{kms}^{-1}$ poloidally, under optimim conditions. Routine error levels are larger. The uncertainty in the poloidal velocity is the dominant contribution to uncertainty in E_r since

[1] Two components (B_r and B_z) of the poloidal magnetic field can in principle be extracted from two lines of sight. With only a single line of sight further constraints on flux surface geometry are required to convert the measurements into a current density.

[2] The plasma E_r contribution can become large in H-mode cases (in particular). In principle E_r can be extracted by employing two views of the injected beam, but the sensitivity is low and the spatial accuracy poor. A set of chords viewing an oppositely directed injector provides the best sensitivity to E_r while also capable of high space resolution.

this term is crossed with the toroidal magnetic field. The best accuracy that can be expected is therefore $25\,\mathrm{kVm}^{-1}$ which corresponds to an accuary in the magnetic field pitch angle of 0.2°. It is shown below, in section 2.2 that this level of uncertainty makes MSE a poor choice for the plasma edge.[3]

1.1.2 Li-Beam

Information about the magnetic field pitch angle in the edge plasma can be obtained from the Zeeman polarised emission of lithium atoms. The polarisation direction is solely dependent on the direction of the magnetic field; there is no interaction from the plasma electrostatic field.

MSE measurements in tokamaks are all based on the measurement of the direction of polarisation of light from a single Stark transition[3, 4, 5, 6]. This polarisation angle is a projection of the magnetic field direction. For Li-beam measurements, however, there are three possible measurement techniques that have been considered for use in tokamaks:

1. Measurement of the polarisation direction of one of the emitted Zeeman transitions. This technique requires polarisation sensitive detection techniques and an oblique viewing geometry in order to be able to resolve the change in the direction of the **B** vector. Optimum sensitivity and space resolution impose somewhat conflicting demands on the beam and line of sight geometry.

2. Measurement of the projection angle between the magnetic field and the diagnostic line-of-sight using the ratio of linear to circular polarised light in the σ transition[7]. This technique makes no special demands on the geometry except that the sensitivy of the measurement decreases to zero as the viewing line becomes parallel to the magnetic field vector. This technique also requires polarisation sensitive detection techniques.

3. Measurement of the projection angle between the magnetic field and the diagnostic line-of-sight using the ratio of intensities in a pair of σ and π transitions[8]. The observation requirements are the same as for the previous technique with the additional constraint that the viewing direction should also not be orthogonal to the magnetic field. The requirement for polarisation sensitive detection is replaced by a need for spectral separation of the Zeeman transitions.[4]

Of these, the last two are the preferred techniques in contemporary implementations.

1.1.3 Edge Charge Exchange

The edge charge exchange system already exists on JET, giving good space resolution in the edge (2 cm). As part of the JET-EP upgrade it will be refurbished with new fibres and optics, the up-down symmetry necessary for the separation of toroidal and poloidal velocites will be restored and new, higher throughput spectrometers with faster, higher efficency detectors will be installed. These improvements will yield better quality measurements of the components of E_r needed to complete study of edge stability.

[3] However, if poloidal flows are believed to be neoclassical then it becomes possible to estimate them to greater accuracy. In this situation the error in E_r would be that arising from the toroidal flow and pressure gradient terms, which are smaller. In this case, the MSE measurements at the edge begin to appear attractive. Alternatively, the use of a diagnostic neutral beam, injecting in the opposite direction to the heating beams, would allow two MSE systems to jointly measure E_r and $J(R)$.

[4] There is still a requirement that the viewing optics, in particular the first mirror, have equal reflectivities for S and P-plane polarisations, or at least that any differences can be measured.

2 Diagnostic Simulations

It is necessary to assess the accuracy required of Li-beam measurements for them to contribute useful information to the calculation of the edge current density profile. In this section the results of such an assessment are presented, based on the JET measurement set and for two possible Li-beam locations. The first option is to leave the Li-beam at its present location at the top of the machine, the second is to move it (or install an additional one) at a midplane port. This assessment follows a similar study done for the DIII-D Li-beam installation[10].

2.1 Methodology of Simulation

The steps involved in this study were as follows:

1. Create a JET equilibrium for an H-mode type discharge having a flat pressure profile in the core with a steep pressure gradient and a peak in current density at the edge.

2. Simulate the measurements that would be obtained from such an equilibrium.

3. Impose random 'measurement' errors on these artifical signals consistent with the anticipated diagnostic accuracies. Reconstruct equilibria, using EFIT, for these sets of measurements and evaluate the spread in current profiles that are deduced.

The starting point was pulse 55923 at 58.21s, during H-mode, just before a type-I ELM crash. It is not possible to run the JET version of EFIT in 'predictive' mode—where a specific current density profile is imposed—due to the way the iron core of the machine is implemented in the code (attempts to circumvent this restriction using internal constraints resulted in inconsistent solutions). Therefore the ESC code[11] was used to establish an equilibrium based on the fixed-boundary solution obtained from the magnetic sensors and a specifically imposed internal current radial distribution.

The output of the ESC code, including idealised synthetic internal measurements, was passed as input to EFIT. An initial fitting run with EFIT was done to remove some small discrepencies between the signals predicted by the two codes. The idealised output from EFIT was taken as the basis for further study.

The idealised signal set was composed of the magnetic signals presently available at JET (PF-coil currents, poloidal field sensors, full flux loops and saddle coils). The signal set also contained MSE measurements from two positions in the core plasma and Li-beam signals for 9 channels of the present upper port system and 9 channels of a postulated outer midplane system. Li-beam signals were generated by moving the position of the existing MSE channels to the required positions and generating the required Green function tables.

From this idealised signal set a number of subordinate sets were created with random errors added to the Li-beam and MSE signals. Additionally, Li-beam channels were selectively turned off to evaluate the effect of each of the two measurement locations, upper or midplane. Batches of such datasets were passed to EFIT and the resulting sets of reconstructed current profiles combined to estimate the uncertainty in $J(R)$ arising from the practical accuracy in the Li-beam measurements.

A simple model for the response of the Li-beam diagnostic was taken. The true measurement of such a system is that of the angle between the LOS and the total **B** direction (the latter two options in section 1.1.2)—B_θ/B_T, which cannot be cast

in the quotient formulation used for the general MSE measurement and currently implemented in the JET EFIT. (With certain approximations it is possible to recast the equations describing the response of the Li-beam system such that they can be implemented within the framework used to model the MSE diagnostic. See Appendix B.) Instead, the midplane system was taken to be a measure of the ratio B_Z/B_T and the upper system the ratio B_R/B_T. For the midplane system this is a good approximation ($B_Z \simeq B_\theta$), but for the upper system the radial field component is only about half of the total poloidal field.

2.2 Results

Figure 1 shows the results of ten EFIT runs with input Li-beam data for a midplane system, with Gaussian random errors of 0.2 degrees added to the the Li-beam points. The simulation shows excellent resolution of the peak in edge cur-

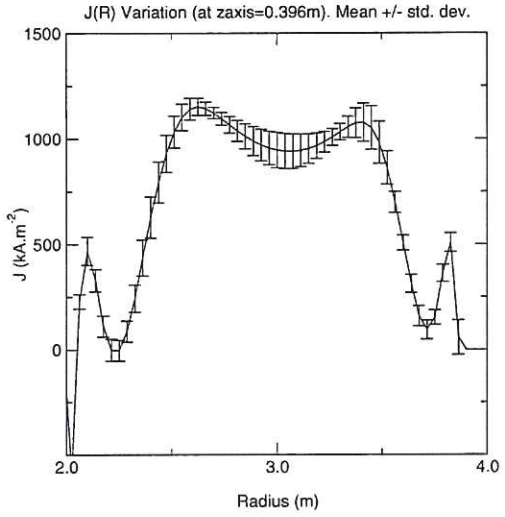

Figure 1: *Current density profile at the midplane, J(R,Z=Zaxis), derived from* EFIT *with midplane measurements from a Li-beam diagnostic with an assumed accuracy of 0.2 degrees. Resulting uncertainty in profile at edge peak (3.825 m) is* $\pm 44\,kA.m^{-2}$.

rent, the error bar in the point at the peak of the edge current peak, at 3.825 m, is $\pm 44\,kA.m^{-2}$. Even if the scatter in the Li-beam data is increased to 0.4 degrees them the uncertainty in the calculation of the edge current peak only rises to $\pm 71\,kA.m^{-2}$. The corresponding plot for Li-beam measurements at the upper port position is shown in figure 2. Here, even with 0.2 degree accuracy on the Li-beam measurements the uncertainty in the magnitude of the edge current rises to $\pm 138\,kA.m^{-2}$.

The results of several simulations are summarised in table 1. The first row of the table shows the edge current values obtained with the idealised (no errors) Li-beam signals from the midplane and upper systems. The following two rows show the effect of adding scatter to the Li-beam data as described, and show the larger uncertainty that occurs with the upper Li-beam. These values are all obtained with the pressure profile unconstrained. The pressure profiles that are obtained in these cases are all mildly peaked, with no strong edge pressure gradients.

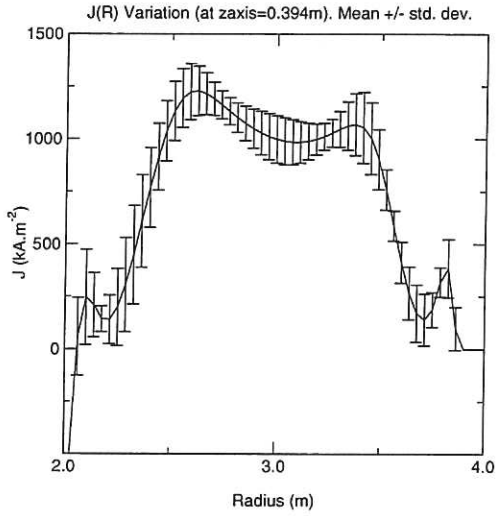

Figure 2: *Current density profile uncertainty with upper Li-beam measurements and an assumed accuracy of 0.2 degrees.Resulting uncertainty in profile at edge peak is* $\pm 138\,kA.m^{-2}$.

The next two rows of the table show the effect of constraining the pressure profile to be 'H-mode like', that is, flat out to $r/a \sim 0.8$ then falling steeply to the boundary. Two cases are calculated, with the core pressure at 50 kPa (appropriate for this shot) and with the core pressure halved. The table shows that there is an effect on the calculated edge current from including the pressure constraint—in part this arises from allowing more freedom in the pressure function (more spline knots), and partly from the details of the pressure profile actually imposed. Including the pressure profile constraint in the case of the upper Li-beam measurements results in an increase in the calculated edge current, bringing the result closer to the 'true' value. The uncertainty in the estimate remains, however, similar. For the case including midplane Li-beam measurements the inclusion of the pressure profile has little influence on the resulting current estimate. In this case, including the incorrect (halved) pressure profile adversely affects the estimated edge current.

2.2.1 Ballooning Calculations

The effect of the different constraints imposed by the Li-beam data, as enumerated in table 1 can be examined in terms of their effects on the ballooning stability estimates of the edge. Selected equilibria from the datasets near to either end of the error ranges were tested with the ballooning stability code IDBALL. Figure 3 shows two such pairs of calculations for the case of 0.2° errors with measurements from either a midplane or an upper Li-beam system. The left column of the figure shows that the range of equilibria computed with the midplane Li-beam data (upper and lower plots) show little variation in the stability boundary. On the other hand, the equilibria computed from the upper Li-beam data show a wide variation, to the extent that it becomes impossible to determine whether or not the plasma has access to second stability.

The pressure gradients in the ballooning plots are calculated from the pressure profiles in the equilibrium. The experimental pressure profiles have larger gradients than are shown by these plots. As mentioned above, including the pressure

σ_γ scatter in Li-beam signals	J, σ_J—resulting J error, kAm^{-2}					
	Midplane			Upper		
-	489			560		
0.2°	508	±44	9%	384	±138	36%
0.4°	570	±71	12%	260	±227	87%
0.2°†	535	±79	15%	516	±173	34%
0.2°‡	311	±43	14%	501	±131	26%
0.2°MSE	530	±168	32%			

† Including pressure constraint
‡ Pressure halved

Table 1: *Summary of simulation results showing the effect of different measurement accuracies and Li-beam positions on the evaluation of the edge current density. The accuracies in the measurement influence both the uncertainty in the edge current and also its absolute value.*

data does have an impact on the equilibrium, but the self-consistent inclusion of an H-mode like pressure profile would require an extension of the present study.

2.2.2 MSE Sensitivity Implications

The final row of table 1 shows the calculation for an edge viewing MSE system, with a measurement accuracy of 0.2°, equivalent to the first row of the table. The calculations for the MSE system are based on an accuracy of 0.2° in the measured polarisation angle. The magnitude of this polarisation angle is roughly half the magnetic pitch angle. The figure for the Li-beam is the accuracy with which the magnetic pitch angle itself is determined, which implies a higher precision in the instrument resolution. This difference accounts for part of the difference in the two calculations, nevertheless, the practical uncertainties in accounting for the influence of E_r on the MSE measurements mean that the figure of 0.2° at the polarimeter cannot be improved.

2.2.3 MSE Edge View Optimisation

The space resolution and spectral isolation of the MSE emission was considered in the design study[9]. Figures 6 and 10 show that there is no viewing position with adequate space resolution and spectral isolation for the very edge plasma. New calculations for ports at positions -11.25° and +11.25° from the injector show that the first of these options suffers from acute spectral overlap, while the other, although more promising, only has a spatial resolution of 5 cm at 3.95 m, worsening rapidly inside the plasma.

3 Options

The options for edge current measurements are the following

Leave the Li-beam in its present position, but improve the beam brightness

Move the Li-beam to the midplane, or install a new diagnostic at this position

Build a high resolution edge MSE system

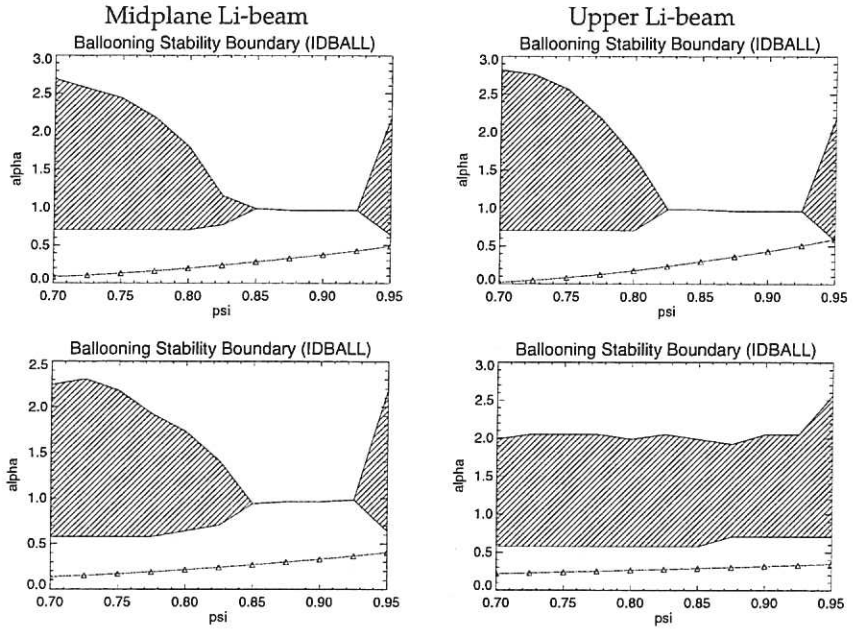

Figure 3: *Ballooning stability boundaries calculated for equilibria constrained by Li-beam measrements: left hand column—midplane Li-beam system; right hand column—upper Li-beam system. 0.2° errors assumed. Upper and lower plots are calculated using equilibria from near the extremes of the error bars in figures 1 and 2. (Shaded area is ballooning unstable, where the shaded area disappear the plasma has access to second stability. Line/triangles shows the actual pressure parameter, α, calculated for the plasma.)*

There are several significant problems with the third option, as discussed above: the relatively poor space resolution achievable with the JET ports, the relatively poor impact on the determination of the edge current and the difficulty of accurately accounting for the plasma E_r in the interpretation of the MSE signals. This option is therefore rejected.

Of the two options for upgrading the Li-beam diagnostic, the installation of a new system at the midplane is preferred since this is shown to be the best position from which to study the plasma edge stability. However, this project requires a significant investment in cash and manpower, and possibly the sacrifice of other diagnostics or systems presently using midplane ports. Nevertheless, in order that such an option can be kept open it is important to state the requirements for optimum measurement accuracy.

3.1 Li-beam Viewing Requirements

As described in [8], the sensitivity of the Li-beam measurement falls to zero in the case that the observation direction lies parallel to the magnetic field. This is also true of the measurement technique being applied at DIII-D[7], using the circular to linear polarised fraction. However, for the line intensity ratio developed in [8] there is a second null in the response for the case of perpendicular viewing. The

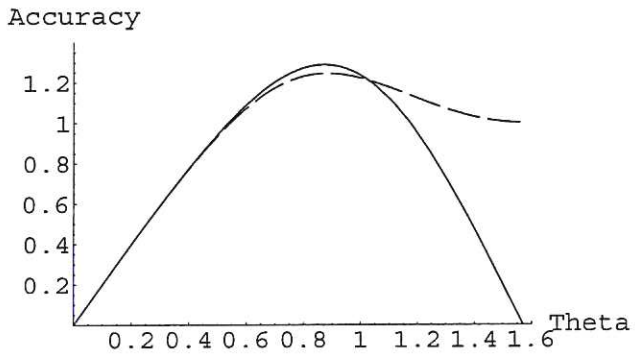

Figure 4: *Figure showing the relative measurement accuracy of a Li-beam diagnostic as a function of the angle θ (in radians) between the line-of-sight and the magnetic field. The accuracy plotted is $\Delta\theta(\theta)$ for a constant $\Delta\xi$. The solid curve is for the measurement scheme used at JET[8] and the dashed curve for the technique used at DIII-D[7]. The difference in the dependence at angles close to perpendicular arises from the angular dependence of the different Zeeman emission features.*

sensitivities of the two techniques are illustrated in figure 4.

Considerations of the accuracy available from different viewing geometries influences the choices of midplane ports for the Li-beam, as illustrated in figure 5, where different deployments of Li-beam and viewing optics are considered. A viewing direction along W-Y is almost parallel to B and offers little sensitivity in the measurement (θ=0.15 in figure 4). A viewing geometry along Z-Y makes an angle of only 10° to the field lines, giving a relative accuracy in the measurement of 0.35 from figure 4. A geometry taking the line X-Z combines the angle between the ports (20°) and the B-field inclination to achieve 30° and hence a relative accuracy of 1.0. A vertical viewing geometry makes an angle of 80° to the magnetic field and hence achieves an accuracy of 0.5 in the JET detection scheme. (For the DIII-D detection scheme, this has a higher accuracy of about 1.0.)

4 Conclusions

A lithium beam diagnostic, deployed on the midplane of JET, would be up to four times more effective in constraining the edge current density profile evaluation than a similar system mounted in the present location, at the top of the machine. (Practical limits on the viewing geometry probably reduce this advantage to a factor of two improvement with the midplane system based on limiter guide tube ports.) Assuming that such a system possessed a sufficiently intense beam, achieving measurement accuracies of 0.2°(0.4% in intensity ratio), then the diagnostic would allow the discrimination of first and second ballooning stability. A lithium beam at the midplane also benefits from the better knowledge of the flux surface orientation (vertical) allowing a direct conversion of the measurements to current density.

The Li-beam technique is superior to an MSE system in JET due to the specific geometries of the vessel ports and the neutral beams. In addition, the insensitivity of the Li-beam technique to the plasma electrostatic field makes it the method of

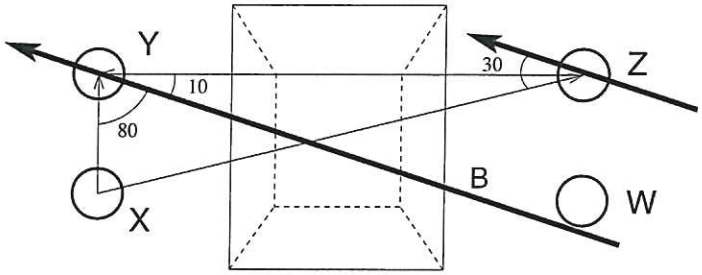

Figure 5: *Viewing geometries for a Li-beam diagnostic using the limiter guide tube (LGT) ports at the midplane, as an example. The condition for the best accuracy is with the viewing line-of-sight at 48° (0.84 radians) to the magnetic field direction. Assuming the normal helicity for JET the field lines at the edge of the plasma are tilted at about 10°. It is important to avoid the viewing geometry W-Y, that is, with the Li-beam in one of the ports and the detection optics in the other, since the viewing LOS lies almost parallel to the magnetic field.*

choice.

To be able to deploy a Li-beam diagnostic on the midplane of JET, two ports will be required. If ports are to be reserved in readiness for such an enterprise then care must be taken to ensure that they possess the optimum geometric arrangements for the measurements.

5 Acknowledgement

This work was funded jointly by the United Kingdom Engineering and Physical Sciences Research Council and by EURATOM.

References

[1] M. C. Zarnstorff, F. M. Levinton, S. H. Batha and E. J. Synakowski, Phys. Plasmas **4** 1097 (1997)

[2] N. C. Hawkes *et al.*, Plasma Phys. Control. Fusion **38** (1996) 1261

[3] F. M. Levinton *et al.*, Rev. Sci. Instrum. **61** (1990) 2914

[4] D. Wroblewski *et al.*, Rev. Sci. Instrum. **61** (1990) 3552

[5] N. C. Hawkes *et al.*, Rev. Sci. Instrum. **70** (1999) 894

[6] R. Jaspers *et al.*, Rev. Sci. Instrum. **72** (2001) 1018

[7] D. M. Thomas, et al., Proc. Workshop on Advanced Diagnostics for Magnetic and Inertial Fusion, Varenna, Italy (2001)

[8] A. A. Korotkov *et al.*, *Line Ratio Method for Measurement of Magnetic Field Vector using Li-Multiplet* ($2\,^2S$–$2\,^2P$) Emission, EFDA-JET-PR(03)19, 2003

[9] N. C. Hawkes, *Design Study of a Motional Stark Effect Diagnostic for JET*, JET-R(96)10, 1997

[10] T. H. Osborne and D. M. Thomas, DIII-D Physics Memo, D3PM 0004, May 2000

[11] L. E. Zakharov and A. Pletzer, Phys. Plasmas **6** (1999) 4393

A Simulation Details

The shot used for the simulation studies is 55923, at 58.2 just before the first type-I ELM. A 65×65 grid was used. The EFIT parameters are given below, for `K55923.T58217_1_d4r`.

Spline basis functions for p' and ff'.

```
KPPFNC  =            6,
KFFFNC  =            6,

KPPKNT  =            4,
PPKNT   = 0.0, 0.25, 0.5, 1.0

KFFKNT  =            6
FFKNT   = 0.0, 0.50, 0.8, 0.95  0.975, 1.0
FFKNT   = 0.0, 0.50, 0.8, 0.95  0.982, 1.0
```

Tensioned splines are not used, but the curvature at the knot points is controlled with a penalty factor

```
FWTXX   =   .001

KCALPA =   9
calpa  =  .01 -.01    0     0     0     0     0     0     0
         -.01  .02  -.01    0     0     0     0     0     0
           0  -.01   .02  -.01    0     0     0     0     0
           0    0   -.01   .02  -.01    0     0     0     0
           0    0     0   -.01   .02  -.01    0     0     0
           0    0     0     0   -.01   .02  -.01    0     0
           0    0     0     0     0   -.01   .02  -.01    0
           0    0     0     0     0     0   -.01   .02  -.01
           0    0     0     0     0     0     0   -.02  -.02
XALPA   =  9*0.0

KCGAMA  =   9,
CGAMA=   1  -1   0    0    0     0    0     0   0
        -1   2  -1    0    0     0    0     0   0
         0  -1   2   -1    0     0    0     0   0
         0   0  -1    2   -1     0    0     0   0
         0   0   0  -0.1  0.2  -0.1   0     0   0
         0   0   0    0  -0.1   0.2 -0.1    0   0
         0   0   0    0    0   -.1   .2   -.1   0
         0   0   0    0    0     0   -1     2  -1
         0   0   0    0    0     0    0    -2   2
XGAMA   =   9*0.0

PCURBD   =  0.0,          Finite edge pressure and current
FCURBD   =  0.0,
```

In cases with the pressure profile included the number of knots in the p' profile was increased as described below. The pressure profile was also included as shown, file `K55923.T58217_1_e4r`.

```
KPPKNT  =            6,
PPKNT   = 0.0, 0.25, 0.5, 0.95, 0.982 1.0

NDOKIN  =    1,
```

```
KPRFIT    =     3,
NPRESS    =     10,
RPRESS    =
 3.0 3.3 3.6 3.73 3.76 3.79 3.82 3.85 3.88 4.01
ZPRESS    =
 0.3 0.3 0.3 0.3 0.3 0.3 0.3 0.3 0.3 0.3
PRESSR    =
   5.e4  5e4 5e4,    5e4,   5e4,   50481.7, 31496.7,   21295.8,
   15942.7,      9947.2,      8141.5,
SIGPRE    =
   1.e4 1e4 1e4 1e4 1e4 1e4 1e4 1e4 1e4 1e4
```

MSE channels 8–16 were used to simulate the edge mid-plane Li-Beam measurements, and channels 17–25 the upper Li-beam position. R, Z coordinates and geometric A-coefficients ($\tan\gamma_m = (B_V A_1 + B_R A_5 + B_T A_6)/(B_V A_4 + B_R A_3 + B_T A_2)$):

	R(m)	Z(m)	A_1	A_2	A_3	A_4	A_5	A_6
Edge Li-Beam	3.78	0.2	1.0	1.0	0.0	0.0	0.0	0.0
	3.79	0.2	1.0	1.0	0.0	0.0	0.0	0.0
	3.80	0.2	1.0	1.0	0.0	0.0	0.0	0.0
	3.81	0.2	1.0	1.0	0.0	0.0	0.0	0.0
	3.82	0.2	1.0	1.0	0.0	0.0	0.0	0.0
	3.83	0.2	1.0	1.0	0.0	0.0	0.0	0.0
	3.84	0.2	1.0	1.0	0.0	0.0	0.0	0.0
	3.85	0.2	1.0	1.0	0.0	0.0	0.0	0.0
	3.86	0.2	1.0	1.0	0.0	0.0	0.0	0.0
Upper Li-Beam	3.25	1.57	0.0	1.0	0.0	0.0	1.0	0.0
	3.25	1.58	0.0	1.0	0.0	0.0	1.0	0.0
	3.25	1.59	0.0	1.0	0.0	0.0	1.0	0.0
	3.25	1.60	0.0	1.0	0.0	0.0	1.0	0.0
	3.25	1.61	0.0	1.0	0.0	0.0	1.0	0.0
	3.25	1.62	0.0	1.0	0.0	0.0	1.0	0.0
	3.25	1.63	0.0	1.0	0.0	0.0	1.0	0.0
	3.25	1.64	0.0	1.0	0.0	0.0	1.0	0.0
	3.25	1.65	0.0	1.0	0.0	0.0	1.0	0.0

B Alternate Li-beam Response Model

The signal recorded by the lithium beam diagnostic is given by the equations 2 and 3 in Appendix C. Making the approximation $|\mathbf{B}| = B_t$ these can be rewritten[5]

$$\frac{\cos(\beta)\sin(\phi)B_r - \sin(\beta)B_z}{B_t} = \sqrt{\frac{C-\kappa\xi}{C+\xi}} - \cos(\beta)\cos(\phi) \tag{1}$$

which can be expressed in the form used by EFIT for the MSE response

$$\tan(\gamma_m) = \frac{B_z A_1 + B_r A_5 + B_t A_6}{B_z A_4 + B_r A_3 + B_t A_2}$$

where $\tan(\gamma_m)$ is replaced by $\sqrt{\frac{C-\kappa\xi}{C+\xi}} - \cos(\beta)\cos(\phi)$ (with C and κ taken as constant[6] independent of $\mathbf{B}$) and

$$\begin{aligned} A_1 &= -\sin\beta \\ A_5 &= \cos(\beta)\sin(\phi) \\ A_2 &= 1 \\ A_3 = A_4 = A_6 &= 0 \end{aligned}$$

The following table compares the typical values of these coefficents to those assumed in the idealised case previously discussed.

	Coefficient			
Midplane	A_5	$\cos(17°)\sin(24°)$	0.39	0
	A_1	$\sin(17°)$	0.29	1.0
Upper	A_5	$\cos(30°)\sin(1.57°)$	0.02	1.0
	A_1	$\cos(1.57°)$	0.5	0

The error in the RHS of equation 1 is governed by the error in $\sqrt{\frac{C-\kappa\xi}{C+\xi}}$ which reduces to the error in ξ for $C \approx 1$ and $\kappa \approx 1$. From section 2.4 of [8] the error in ξ is given by

$$\Delta\xi = (1+\xi)\sqrt{\frac{\xi}{(N_\Sigma)}}.$$

Under optimum conditions, during the peak of the emission from a lithum flake, of order 10^4 counts were obtained in the spectrum in one time window, yielding an error in ξ of 0.004 (0.4%). This is comparable to the typical error in $\tan(\gamma_m)$ assumed of 0.2°or 0.0035 radians.

Repeating the study of section 2.2 yields a modified version of table 1.

Scatter in Li-beam signals	J, σ_J—resulting J error, kAm^{-2}					
	Midplane			Upper		
0.2%	480	±80	17%	439	±68	15%
0.4%	404	±165	41%	417	±257	62%
0.8%	483	±388	80%	330	±311	94%

In these results there is less than a factor of two improvement in accuracy obtained with the edge viewing system compared to the upper system with 0.4% errors on the measurements. At other error levels this improvement is reduced or even reversed. This reduction arises as a result of the relatively large value of the toroidal

[5]This approximation is valid if $B_z/2B_t \ll \tan(\beta)/\sin(\phi)$

[6]Corresponding to an ideal mirror, $k = 1$

viewing angle, $\phi \approx 24°$, which is set by the likely constraints of using limiter guide tubes for the beam and viewing optics. Improvements would be achieved by reducing ϕ (moving the viewing optics further from the Li-beam) and increasing β. A view from a lower port would perhaps be more favourable. The improvements continue in these simulations as β is increased to 90°, where the idealised case of table 1 is recovered. However, these simulations neglect the increase in the error in the $\tan(\gamma_m)$ substitute, which becomes large[7] near $\beta = 90$.

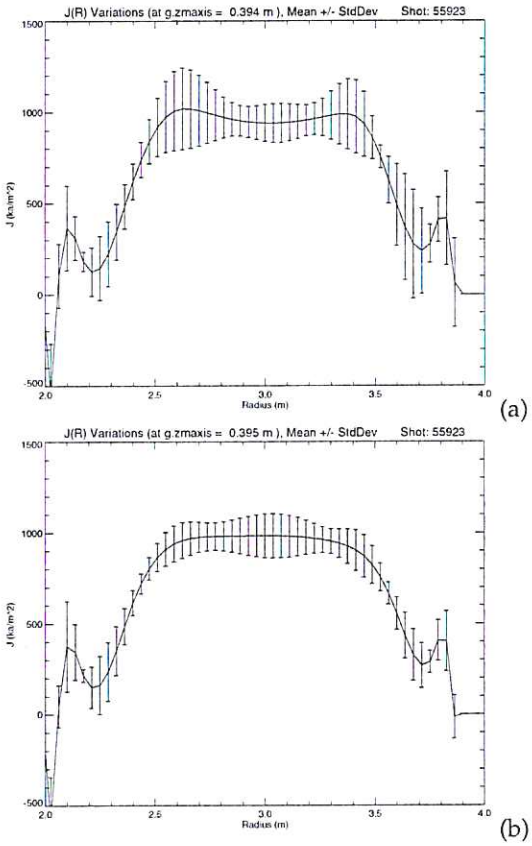

Figure 6: *Current density profile uncertainty with upper Li-beam measurements and an assumed accuracy of 0.4%. (a) upper beam and viewing system, (b) midplane system.*

[7] This is equivalent to the vanishing sensitivity as $\beta \to 90°$ in [8].

C Derivation of Li-beam Response Equations

The Li-beam response functions can be expressed in a compact form based on a Stoke's vector analysis. The Stokes vectors for the Zeeman split Li-beam emission are [7],

$$\begin{matrix} \pi \\ \left\{ \begin{array}{c} \frac{\sin^2(\theta)}{2} \\ \frac{\sin^2(\theta)\cos(2\gamma)}{2} \\ \frac{\sin^2(\theta)\sin(2\gamma)}{2} \\ 0 \end{array} \right\} \end{matrix} \quad \begin{matrix} \sigma+ \\ \left\{ \begin{array}{c} \frac{1+\cos^2\theta}{4} \\ -\frac{\sin^2(\theta)\cos(2\gamma)}{4} \\ -\frac{\sin^2(\theta)\sin(2\gamma)}{4} \\ \frac{\cos(\theta)}{2} \end{array} \right\} \end{matrix} \quad \begin{matrix} \sigma- \\ \left\{ \begin{array}{c} \frac{1+\cos^2\theta}{4} \\ -\frac{\sin^2(\theta)\cos(2\gamma)}{4} \\ -\frac{\sin^2(\theta)\sin(2\gamma)}{4} \\ -\frac{\cos(\theta)}{2} \end{array} \right\} \end{matrix}$$

with the angles θ and γ defined according to figure 7. Applying a Müller matrix

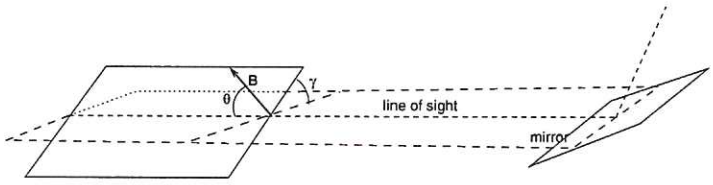

Figure 7: *Definition of the viewing angles for the Stokes vector description of the Zeeman emission from a Li-beam. γ is the tilt angle of the plane containing the magnetic field, θ is the angle between the diagnostic line-of-sight and the magnetic field.*

for the reflection by a mirror with a relative reflectivity for the P polarised light of k, and allowing for the enhancement of the π emission by a factor C (according to [8]) due to atomic physics effects, the intensity ratio can be reduced to

$$\begin{aligned} \xi &= \frac{CJ_\pi}{J_{\sigma+} + J_{\sigma-}} \\ &= \frac{C\sin^2(\theta)}{\cos^2(\theta) + \kappa} \end{aligned} \tag{2}$$

with

$$\kappa = \frac{k + \tan^2(\gamma)}{1 + k\tan^2(\gamma)}$$

(in accordance[8] with equations 2.3 and 2.4 of [8]).

Expressions for the angles γ and θ can be derived from the instrumental geometry to give,

$$\cos(\theta) = \frac{\cos(\beta)B_r\sin(\phi) + \cos(\beta)B_t\cos(\phi) - \sin(\beta)B_z}{|\mathbf{B}|} \tag{3}$$

while $\tan(\gamma)$ is derived from [8], Appendix 2 recognising that $e_1.n = \sin(\gamma)$ and $e_2.n = \cos(\gamma)$).

$$\tan(\gamma) = \frac{-B_r\sin(\beta)\sin(\phi) - B_t\sin(\beta)\cos(\phi) - B_z\cos(\beta)}{B_r\cos(\phi) - B_t\sin(\phi)} \tag{4}$$

[8]Note that γ is defined as in reference [7] but differently from reference [8]. Here γ denotes the angle between the plane containing the **B** vector and the mirror P plane (in [8] it is the angle to the mirror S plane).